

# Simulation of the Buxton-Clarke Model for Organic Photovoltaic Cells

J.W. Jerome

Department of Mathematics  
Northwestern University  
Evanston, IL 60208 USA

Email: jwj@math.northwestern.edu

M.A. Ratner and J.D. Servaites

Departments of Chemistry and  
Materials Science and Engineering  
Northwestern University  
Evanston, IL 60208 USA

C.-W. Shu and S. Tan

Division of Applied Mathematics  
Brown University  
Providence, RI 02912 USA

**Abstract**—Modeling of organic photovoltaic (OPV) cells can be achieved by adaptation of drift-diffusion models. Replacement of traditional crystalline solid state materials by organic materials leads to much lower carrier mobility and to a new carrier, the exciton, which is a bound electron-hole pair. The Buxton-Clarke model includes electrons, holes, and excitons, together with generation, dissociation, and recombination mechanisms connecting these carriers, partially induced by device illumination. Device materials consist of a polymer:fullerene blend, poly(3-hexylthiophene): 6,6-phenyl C61-butyric acid methyl ester (P3HT:PCBM). In this article, the model is used to simulate an active layer of 20 nm; results include I-V curves and carrier current densities.

## I. INTRODUCTION

Organic solar cells are the topic of extensive current research. However, their relatively low efficiency [1] is a major factor limiting their practical use at this time. This paper reports the simulation of polymer:fullerene, poly(3-hexylthiophene): 6,6-phenyl C61-butyric acid methyl ester (P3HT:PCBM), materials, including the determination of current-voltage (I-V) curves, through classical device modeling approaches, via the Buxton-Clarke model [2]. Three carrier types are identified: electrons, holes, and excitons, which are bound electron-hole pairs. They are simulated through carrier continuity equations, self-consistently coupled to Poisson's equation for the electric potential. An early drift-diffusion model for bulk heterojunction cells was discussed in [3], which employs a rate equation for excitons in place of a reaction/diffusion equation. This modeling was continued in [4], [5]. For a mathematical study based on [4], see [6]. An important reference for the Schottky boundary conditions used in this paper is [7].

## II. CHARACTERISTICS OF ORGANIC CELLS

Theoretical efficiency limits were established by Shockley and Queisser for silicon p-n junction solar cells in [8]. Subsequent studies of power conversion efficiency  $\eta$  have built upon this analysis. One can define  $\eta$  as the ratio,  $J_{\max}V_{\max}/P_{\text{solar}}$ , where the denominator represents solar radiation power, and the numerator represents optimal device power. It has been found that critical energy levels are assumed by the lowest unoccupied molecular orbitals (LUMO), in both

the polymer donor (D) and the fullerene acceptor (A). The offset energy parameter is defined as:

$$E_{\text{LLO}} = \left| E_{\text{LUMO(A)}} - E_{\text{LUMO(D)}} \right|.$$

If the exciton binding energy is overcome at the D:A interface, in [1] it was shown that OPV efficiencies of greater than 10% can be achieved by appropriate optimization of the donor bandgap energy  $E_g$ , the series resistance  $R_s$ , and certain other device parameters, when  $E_{\text{LLO}} \approx .3 - .4$  eV. Fig. 1 indicates the limiting power efficiency as a function of  $E_{\text{LLO}}$ ; here, we have made assumptions regarding charge density efficiency. Regarding terminology, note that the terms HOMO (highest occupied molecular orbital) and LUMO are not strictly accurate, but are used in accordance with the literature. To use more accurate terms, "HOMO" should be replaced by "ionization potential" and "LUMO" replaced by "electron affinity." For further details, see [1], [9].

## III. MODEL

In the following system, the quantities  $D$  and  $G$  are exciton dissociation and photo-generation rates, respectively. Recombination of electrons and holes is expressed via  $R(n, p)$  and  $R(X)$  expresses relaxation of excitons. Further,  $E$  is the electric field,  $q$  is the charge unit,  $T_0$  is the ambient temperature,  $t$  is time,  $k$  is Boltzmann's constant,  $\epsilon$  is the dielectric constant, and the carrier mobilities are represented by  $\mu_n, \mu_p$ . The pseudo-mobility of excitons, with adjusted units of mobility, is denoted  $\mu_X$ . The Einstein relations, relating mobility and diffusion coefficients, are incorporated. The device material consists of two layers of different relative dielectric constants and mobilities (see the next section). Boundary and initial conditions are prescribed. We state the system initially as a time dependent multi-dimensional system. In the following section, we specialize to one dimension, corresponding to the thickness of the active layer.

The Gauss law for the electric force is expressed in the first equation of the system. The next three equations are standard continuity equations for the carriers. Specifically,  $n, p, X$ , which are the densities of electrons, holes, and excitons, resp., and the electric potential  $\phi$  evolve as:

$$\nabla \cdot (\epsilon \nabla \phi) = -q(p - n), \quad E = -\nabla \phi \quad (1)$$

$$\begin{aligned} \frac{\partial n}{\partial t} &= D(\nabla \phi, X) - R(n, p) \\ -\frac{1}{q} \nabla \cdot [qn\mu_n \nabla \phi - kT_0\mu_n \nabla n] & \end{aligned} \quad (2)$$

$$\begin{aligned} \frac{\partial p}{\partial t} &= D(\nabla \phi, X) - R(n, p) \\ -\frac{1}{q} \nabla \cdot [-qp\mu_p \nabla \phi - kT_0\mu_p \nabla p] & \end{aligned} \quad (3)$$

$$\begin{aligned} \frac{\partial X}{\partial t} &= G - D(\nabla \phi, X) + \frac{1}{4} R(n, p) \\ -R(X) + \frac{1}{q} \nabla \cdot [kT_0\mu_X \nabla X] & \end{aligned} \quad (4)$$

#### IV. GEOMETRY AND PARAMETERS

A one-dimensional model is used, with length (device thickness)  $L = 20$  nm. This incorporates an implicit assumption relative to planes perpendicular to the direction through the active layer: within any plane, the changes in physical properties are negligible with respect to changes in the orthogonal direction. It follows that  $\nabla := d/dx$ . The illumination site is at  $x = 0$  and the electron collection site at  $x = L$ . The donor material occupies the region  $(0, L/2)$  and the acceptor region occupies  $(L/2, L)$ .

- 1) The relative dielectric constant for the donor material is taken as  $\epsilon_D = 6.5$  [10, p. 56], while the relative dielectric for the acceptor material is  $\epsilon_A = 3.9$ ;
- 2) average lifetime of an exciton [2, p. 19]:  $\tau_X = 1 \mu\text{s}$ ;
- 3) exciton pseudo-mobility, with adjusted units of mobility [2, p. 19]:  $\mu_X = 3.86 \times 10^{-5} \text{ cm}^2/\text{V/s}$ ;
- 4) maximum electron and hole mobility [11, p. 866]:  $\mu_{0,n} = 7.7 \times 10^{-5} \text{ cm}^2/\text{V/s}$ ,  $\mu_{0,p} = 5.1 \times 10^{-5} \text{ cm}^2/\text{V/s}$ ;
- 5) photon flux [12, p. 1]:  $\Gamma_0 = 4.31 \times 10^{17}/\text{cm}^2/\text{s}$ ;
- 6) absorption coefficient [13, sec. 3.4]:  $\alpha_0 = 2 \times 10^5/\text{cm}$ ;
- 7) exciton pair characteristic length separation [2, p. 16]:  $a = 1$  nm;
- 8) exciton pair binding energy [2, p. 19]:  $E_B = .5$  eV;
- 9) field dependent mobility parameter [2, p. 19]:  $\gamma = 5 \times 10^{-3} \text{ cm}^{1/2}/\text{V}^{1/2}$ .

#### V. EXPRESSIONS

- 1) Poole-Frenkel mobility expressions for both electrons and holes:  $\mu = \mu_0 \exp(\gamma|E|^{1/2})$ . Note that  $\mu = \mu_n$  or  $\mu = \mu_p$ , depending on the value of  $\mu_0$  defined in the previous section.
- 2) Recombination:  $R(n, p) = \frac{q(\mu_n + \mu_p)np}{\epsilon} = \gamma_r np$  [2, p. 17]. Here, we have defined  $\gamma_r$  to be the factor of  $np$ .
- 3) Onsager dissociation [14]:  $D(E, X) =$

$$\frac{3\gamma_r}{4\pi a^3} \exp[-E_B/(kT_0)] \Phi(b(|E|))X,$$

where  $b(|E|)$  is given by

$$b(|E|) = (q^3|E|)/(8\pi\epsilon k^2 T_0^2),$$

and  $\Phi$  is given in terms of the Bessel function  $J_1$  of order one by

$$\Phi(u) = J_1(2\sqrt{-2u})/\sqrt{-2u}, \quad u \mapsto b(|E|).$$

- 4) Exciton relaxation:  $R(X) = \frac{X}{\tau_X}$  [2, p. 17].
- 5) Carrier generation;  $G(x) = \alpha_0 \Gamma_0 \exp(-\alpha_0 x)$  [13, sec. 3.4]. ( $x$  denotes the distance from the illumination site.)
- 6) Coulomb radius:  $r_C = \frac{q^2}{4\pi\epsilon kT_0}$  [7, eq. (1)]. Here,  $\epsilon_0$  is the vacuum dielectric constant.

#### VI. BOUNDARY CONDITIONS

- 1) Exciton homogeneous Dirichlet conditions.
- 2) Hole boundary conditions: Zero flux at  $x = L$ ; Schottky barrier condition at  $x = 0$  (described below).
- 3) Electron boundary conditions: Zero flux at  $x = 0$ ; Schottky barrier condition at  $x = L$ .
- 4) Various values of the potential bias can be assigned. Many of the computations were carried out at  $\phi_0 = .7\text{V}$  and  $\phi_L = 0$ .
- 5) Schottky Dirichlet boundary condition (applicable to electrons and holes) The barrier concentration is field dependent, and is given in [7, eq. (11)]. This equation states the concentration as:

$$n_0 = 4\psi^2 N_0 \exp(f^{1/2}),$$

where  $f$  and  $\psi$  are given as:

$$f = \frac{q|E|r_C}{kT_0},$$

$$\psi(f) = f^{-1} + f^{-1/2} - f^{-1}(1 + 2f^{1/2})^{1/2}.$$

Instability occurs for  $f = 0$ .  $N_0$  is the surface density and is a critical parameter [7].

#### VII. NUMERICAL METHOD

We began the evolution at zero values of the carriers and used time accurate Runge-Kutta time stepping to reach steady state. The convective terms (first order spatial derivative terms) in the equations (1)-(4) were discretized by the fifth order weighted essentially non-oscillatory (WENO) method [15], which combines steep-gradient tracking with smooth solution resolution. The second derivative terms were discretized by standard central differences. The combined algorithm is stable in the presence of sharp gradients or discontinuities in the solution and is high order accurate.

#### VIII. RESULTS

For the displayed figures,  $N_0$  has been set to  $10^{18}/\text{cm}^3$  (except Fig. 10). It was found that instability occurs beyond  $10^{19}/\text{cm}^3$ , when the bias across the device is less than .7V. This is the potential difference selected, except in Figures 8–10. In Fig. 2, we display the electron and hole density profiles. The exciton density profile is portrayed in Fig. 3 and the electric potential in Fig. 4. In Fig. 5, we display the electric field profile, and in Fig. 6, the electron and hole current densities.

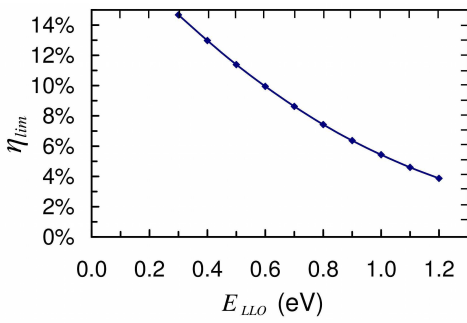


Fig. 1. Practical OPV efficiency limit vs  $E_{LLO}$  (LUMO-LUMO offset). Results assume that the exciton binding energy is overcome at the D:A interface. Reprinted with permission from Reference [1], Copyright 2009, American Institute of Physics.

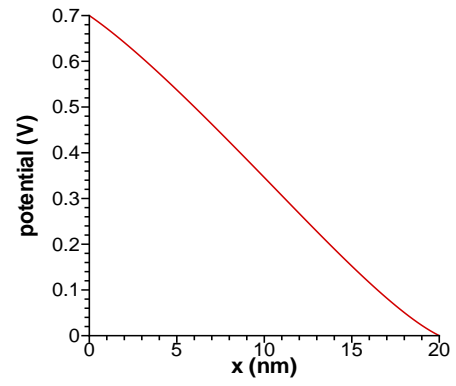


Fig. 4. Steady-state potential profile.

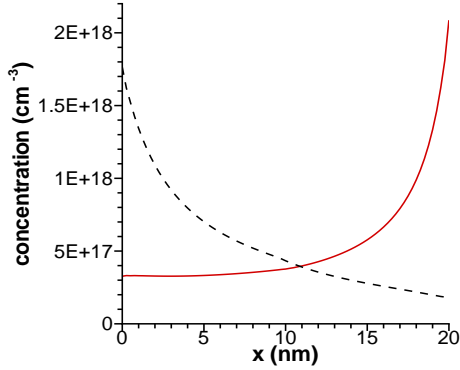


Fig. 2. Steady-state electron and hole density profiles. Solid: Electron density; Dashed: Hole density.

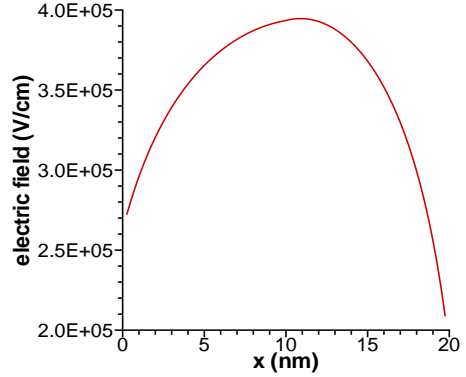


Fig. 5. Steady-state electric field profile.

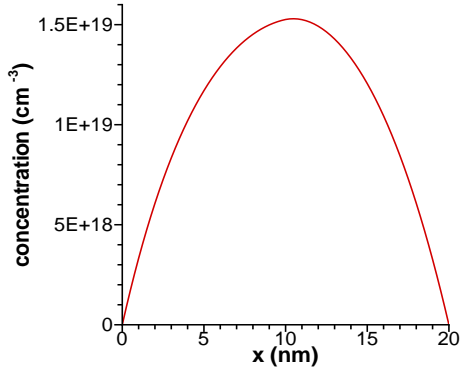


Fig. 3. Steady-state exciton density profile.

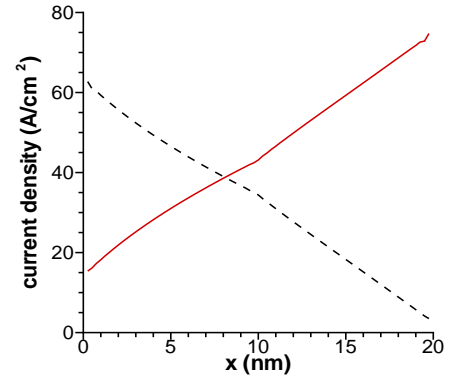


Fig. 6. Steady-state current density profiles. Solid: Electron current density; Dashed: Hole current density.

Time evolution of total current density is portrayed in Fig. 7 and, for comparison, for a higher potential bias (1.4V in Fig. 8). In Fig. 9, the steady-state I-V curve is shown, and in Fig. 10, for  $N_0 = 10^{19}/\text{cm}^3$ . It was found that the exciton density reaches steady state in 2-3  $\mu\text{s}$ , whereas the electron and hole densities attain equilibrium much faster, on the order of .02 $\mu\text{s}$  for a bias of .7V. This increases to .1 $\mu\text{s}$  for a bias of 1.4V. A possible explanation is that the exciton dissociation rate is smaller, by a factor  $10^{-3} - 10^{-4}$ , than recombination and convection/diffusion.

## IX. DARK CURRENT

Comparison simulations were carried out to determine current density information in the absence of illumination. Fig. 11 indicates a 26.3% reduction in current for the 20 nm device with respect to the illuminated device.

## ACKNOWLEDGMENTS

The first author was partially supported by NSF gr. DMS-0935967. The second and third authors were supported by the Argonne-Northwestern Solar Energy Research (ANSER),

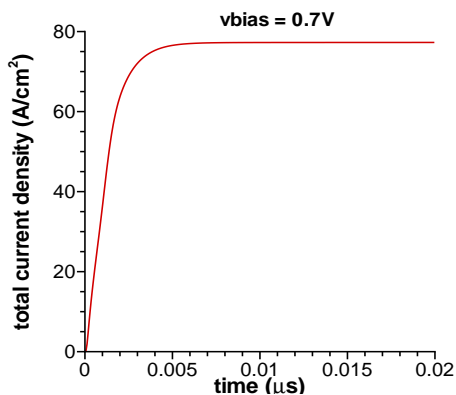


Fig. 7. Time evolution of total current density at .7V vbias.

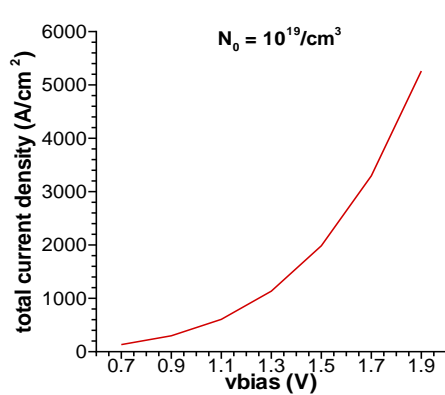


Fig. 10. Steady-state I-V curve for  $N_0 = 10^{19}/\text{cm}^3$ .

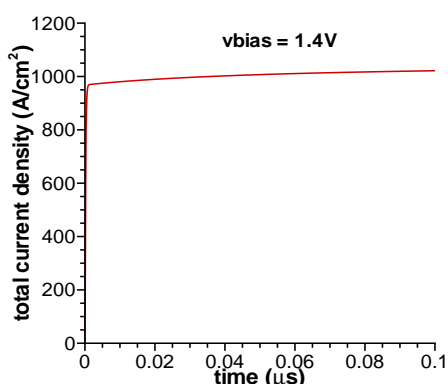


Fig. 8. Time evolution of total current density at 1.4V vbias.

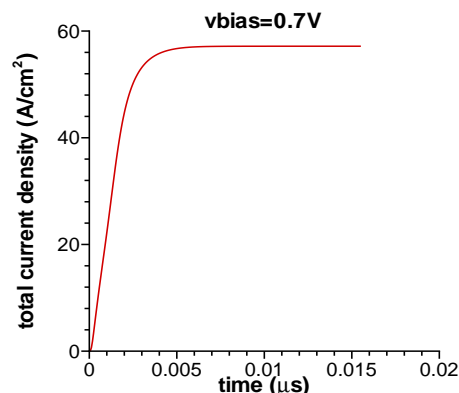


Fig. 11. Dark current evolution for a 20 nm device

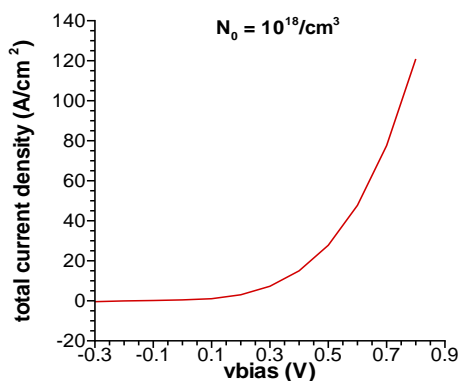


Fig. 9. Steady-state I-V curve for  $N_0 = 10^{18}/\text{cm}^3$ .

and the Northwestern University Materials Research Science & Engineering Center (MRSEC). The fourth and fifth authors were partially supported by ARO gr. W911NF-08-1-0520 and NSF gr. DMS-0809086.

#### REFERENCES

- [1] J.D. Servaites, M.A. Ratner, and T.J. Marks, Practical efficiency limits in organic photovoltaic cells: functional dependence of fill factor and external quantum efficiency. *Appl. Phys. Lett.* **95** (2009) art. no. 163302.
- [2] G.A. Buxton and N. Clarke, Computer simulation of polymer solar cells. *Modelling Simul. Mater. Sci. Eng.* **15** (2007) 13–26.
- [3] L.J.A. Koster, E.C.P. Smits, V.D. Mihailetschi, and P.W.M. Blom, Device model for the operation of polymer/fullerene bulk heterojunction solar cells. *Phys. Rev. B* **72** (2005) art. no. 085205.
- [4] I. Hwang and N.C. Greenham, Modelling photocurrent transients in organic solar cells. *Nanotechnology* **19** (2008) art. no. 424012.
- [5] I. Hwang, C.R. McNeill, and N.C. Greenham, Drift-diffusion modelling of photocurrent transients in bulk heterojunction solar cells. *Jour. Appl. Phys.* **106** (2009) art. no. 094506.
- [6] C. de Falco, R. Sacco, and M. Verri, Analytical and numerical study of photocurrent transients in organic polymer solar cells. *CMAME* **199** (2010), 1722–1732.
- [7] J.C. Scott and G.G. Malliaras, Charge injection and recombination at the metal-organic interface. *Chemical Physics Letters* **299** (1999), 115–119.
- [8] W. Shockley and H.J. Queisser, Detailed balance limit of efficiency of  $p-n$  junction solar cells. *J. Appl. Phys.* **32** (1961), 510–519.
- [9] J.D. Servaites, S. Yeganeh, T.J. Marks, and M.A. Ratner, Efficiency enhancement in organic photovoltaic cells: consequences of optimizing series resistance. *Adv. Funct. Mater.* **20** (2010), 97–104.
- [10] M. Estrada, I. Mejia, A. Cerdaira, and B. Iñiguez, MIS polymeric structures and OTFTs using PMMA on P3HT layers. *Solid-State Electronics* **52** (2008), 53–59.
- [11] G. Li, V. Shrotriya, J. Huang, Y. Yao, T. Moriarty, K. Emery, and Y. Yang, High efficiency solution processable polymer photovoltaic cells by self-organization of polymer blends. *Nature Materials* **4** (2005), 864–868.
- [12] D. Dennler, M.C. Scharber, and C.J. Brabec, Polymer-fullerene bulk heterojunction solar cells. *Adv. Mater.* **21** (2009), 1–16.
- [13] A.L. Fahrenbruch and R.H. Bube, *Fundamentals of Solar Cells*, Elsevier Science, 1983.
- [14] J. Barker, C. Ramsdale, and N. Greenham, Modeling the current-voltage characteristics of bilayer polymer photovoltaic devices. *Phys. Rev. B* **67** (2003) art. no. 075205.
- [15] G. Jiang and C.-W. Shu, Efficient implementation of weighted ENO schemes, *J. Comput. Phys.* **126** (1996), 202–228.